Absolute and Relative Rate Constants for the Reactions $CH_3C(O)O_2$ + NO and $CH_3C(O)O_2$ + NO_2 and Thermal Stability of $CH_3C(O)O_2NO_2$

Jens Sehested,*,† Lene Krogh Christensen, Trine Møgelberg,‡ and Ole J. Nielsen*,§

Atmospheric Chemistry, Plant Biology and Biogeochemistry Department, Risø National Laboratory, DK-4000 Roskilde, Denmark

Timothy J. Wallington*,|| and Andrei Guschin

Ford Research Laboratory, SRL-3083, Ford Motor Company, P.O. Box 2053, Dearborn, Michigan 48121-2053

John J. Orlando⊥ and Geoffrey S. Tyndall▽

Atmospheric Chemistry Division, National Center for Atmospheric Research, P.O. Box 3000, Boulder, Colorado 80307

Received: September 4, 1997; In Final Form: December 2, 1997

A pulse-radiolysis system was used to measure absolute rate constants for the reactions of $CH_3C(O)O_2$ radicals with NO and NO_2 at 295 K and 1000 mbar total pressure of SF_6. When the rate of formation and decay of NO_2 using its absorption at 400.5 and 452 nm were monitored, the rate constants $k(CH_3C(O)O_2 + NO) = (2.0 \pm 0.3) \times 10^{-11}$ and $k(CH_3C(O)O_2 + NO_2) = (1.0 \pm 0.2) \times 10^{-11}$ cm^3 molecule^{-1} s^{-1} were determined. Long path-length Fourier transform infrared spectrometers were used to study the rate-constant ratio $k(CH_3C(O)O_2 + NO)/k(CH_3C(O)O_2 + NO_2)$ in 6−700 Torr total pressure of N_2 diluent at 243−295 K. At 295 K in 700 Torr of N_2 diluent $k(CH_3C(O)O_2 + NO)/k(CH_3C(O)O_2 + NO_2) = 2.07 \pm 0.21$. The results are discussed in the context of the atmospheric chemistry of acetylperoxy radicals.

1. Introduction

Acetyl peroxy radicals, $CH_3C(O)O_2$, are formed during the atmospheric degradation of oxygenated organic compounds such as acetaldehyde, acetone, and methylglyoxal and react with HO_2, NO, NO_2, or other peroxy radicals ($R'O_2$):

$$CH_3C(O)O_2 + HO_2 \rightarrow \text{products} \quad (1)$$

$$CH_3C(O)O_2 + NO \rightarrow CH_3C(O)O + NO_2 \quad (2)$$

$$CH_3C(O)O_2 + NO_2 + M \rightleftharpoons CH_3C(O)O_2NO_2 + M \quad (3,-3)$$

$$CH_3C(O)O_2 + R'O_2 \rightarrow \text{products} \quad (4)$$

Reaction 3 forms $CH_3C(O)O_2NO_2$ (peroxyacetyl nitrate or PAN), which has sufficient stability toward thermal decomposition in the free troposphere to be transported over long distances from urban high-NO_x areas to remote low-NO_x areas. The efficiency of such long-range transport is determined by the rate constants of reactions 1−4, the concentrations of HO_2, NO, NO_2, and other peroxy radicals ($R'O_2$), and the thermal stability of PAN.

Moortgat et al.,[1,2] Roehl et al.,[3] and Villenave et al.[4] determined k_1 to be $4.3 \times 10^{-13} \exp(1040/T)$ cm^3 molecule^{-1} s^{-1},[2] and k_4 to be $2.8 \times 10^{-12} \exp(530/T)$ ($R'O_2 = CH_3C(O)O_2$),[1] 1.4×10^{-11} ($R'O_2 = CH_3O_2$, 298 K),[1] 1.0×10^{-11} ($R'O_2 = CH_3O_2$, 298 K),[4] and 1.0×10^{-11} cm^3 molecule^{-1} s^{-1} ($R'O_2 = C_2H_5O_2$, 298 K).[4] k_3 was studied by Bridier et al.,[5] Addison et al.,[6] and Basco and Parmar.[7] The rate constants reported by Addison et al. and Basco and Parmar are a factor of 2−3 lower than reported by Bridier et al. As discussed elsewhere, the study of Bridier et al.[5] was more comprehensive than those of Addison et al.[6] and Basco and Parmer,[7] and the data by Bridier et al. are considered more reliable. Bridier et al.[5] report $k_3 = 9.6 \times 10^{-12}$ cm^3 molecule^{-1} s^{-1} at 298 K and 760 Torr total pressure of N_2.

Recently, two absolute studies of k_2 have been reported.[10,11] At room temperature Villalta and Howard[11] measured $k_2 = (2.0 \pm 0.3) \times 10^{-11}$ while Maricq and Szente[10] report $k_2 = (1.4 \pm 0.2) \times 10^{-11}$ cm^3 molecule^{-1} s^{-1}. The objective of the present study is to improve our understanding of the reactions of $CH_3C(O)O_2$ with NO and NO_2. We have measured absolute values of k_2 and k_3 using pulse radiolysis coupled with time-resolved UV absorption spectroscopy employing two different chemical systems. The FTIR spectrometer systems at Ford Motor Company and the National Center for Atmospheric Research (NCAR) were used to measure the rate constant ratio k_2/k_3 and the thermal stability of $CH_3C(O)O_2NO_2$.

2. Experimental Section

The three different experimental systems used for this work are described in detail elsewhere[12−15] and are discussed briefly here. The uncertainties reported in this paper are two standard deviations unless otherwise stated. Standard error propagation methods were used to calculate combined uncertainties.

2.1. Pulse Radiolysis System. $CH_3C(O)O_2$ radicals were generated by radiolysis of either $CH_3CHO/O_2/CO_2/NO_x$ or CH_3-

* To whom correspondence should be addressed.
† E-mail: jens.sehested@risoe.dk.
‡ Present address: Danish Institute of Fundamental Metrology, Building 307, Anker Engelunds Vej 1, DK-2800 Lyngby, Denmark.
§ E-mail: ole-john.nielsen@risoe.dk.
|| E-mail: twalling@ford.com.
⊥ E-mail: orlando@acd.ucar.edu.
▽ E-mail: tyndall@acd.ucar.edu.

S1089-5639(97)02881-8 CCC: $15.00
Published on Web 02/12/1998

$CHO/O_2/SF_6/NO_x$ gas mixtures in a 1-L stainless steel reactor by a 30-ns pulse of 2-MeV electrons from a Febetron 705B field-emission accelerator. The radiolysis dose, referred to herein as a fraction of the maximum dose achievable, was varied by insertion of stainless steel attenuators between the accelerator and the chemical reactor. The analyzing light was obtained from a pulsed Xenon arc lamp and reflected in the reaction cell by internal White-type optics. The length of the cell is 10 cm, and the optical path length for the analysis light was 120 cm. The analyzing light was monitored by a photomultiplier attached to a monochromator operated at a spectral resolution of 0.8 nm. All transients were results of single-pulse experiments.

CO_2 or SF_6 was used as diluent gas. Radiolysis of CO_2 and SF_6 produces oxygen and fluorine atoms, respectively:

$$CO_2 \xrightarrow{\text{2-MeV e}^-} CO + O \quad (5)$$

$$SF_6 \xrightarrow{\text{2-MeV e}^-} F + \text{products} \quad (6)$$

CO_2 or SF_6 was always present in excess to minimize the relative importance of direct radiolysis of other compounds in the gas mixtures.

The O-atom yield following radiolysis of CO_2 was determined using the absorbance of ozone at 254 nm following radiolysis of mixtures of 50 mbar of O_2 and 950 mbar of CO_2.

$$O + O_2 + M \rightarrow O_3 + M \quad (7)$$

The filled circles in Figure 1A show the absorbance after the formation of ozone had ceased as a function of the radiolysis dose. As seen from this figure, the absorbance is proportional to the radiolysis dose. The slope is 0.441 ± 0.021. Using $\sigma_{254\ nm}(O_3) = 1.15 \times 10^{-17}$ cm^2 molecule^{-1} [16] we derive an O atom yield of $(7.75 \pm 0.54) \times 10^{14}$ cm^{-3} at full dose and 1000 mbar of CO_2. The error includes statistical uncertainty in the slope of the data in Figure 1A and a 5% systematic uncertainty associated with the ozone absorption cross section.

The fluorine atom yield was determined by two different methods: first, by measuring the yield of CH_3O_2 radicals following radiolysis of mixtures of 10 mbar CH_4, 40 mbar O_2, and 950 mbar SF_6,

$$F + CH_4 \rightarrow CH_3 + HF \quad (8)$$

$$CH_3 + O_2 + M \rightarrow CH_3O_2 + M \quad (9)$$

and second, by measuring the loss of NO_2 following radiolysis of mixtures of 0.5 mbar of NO_2 and 999.5 mbar of SF_6,

$$F + NO_2 + M \rightarrow FNO_2 + M \quad (10)$$

The maximum transient absorbance at 240 and 260 nm ascribed to CH_3O_2 radicals is plotted in Figure 1A, while the changes in absorbance at 400.5 and 452 nm due to loss of NO_2 via reaction 10 are shown in Figure 1B. As seen from Figure 1, the absorbance is proportional to the radiolysis dose up to 42% of maximum dose. At higher doses the absorbance falls below that expected from extrapolation of the low-dose data. We ascribe this to loss of radicals via unwanted radical−radical reactions at high doses. Based on an optical path length of 120 cm, the slopes of the straight lines through the low-dose data in Figure 1, 0.712 ± 0.014 (CH_3O_2, 240 nm); 0.494 ± 0.011 (CH_3O_2, 260 nm); -0.1040 ± 0.0044 (NO_2, 400.5 nm); -0.0780 ± 0.0015 (NO_2, 452 nm); and $\sigma_{240nm}(CH_3O_2) = (4.42 \pm 0.44) \times 10^{-18}$,[9] $\sigma_{260nm}(CH_3O_2) = (3.18 \pm 0.32) \times 10^{-18}$,[9]

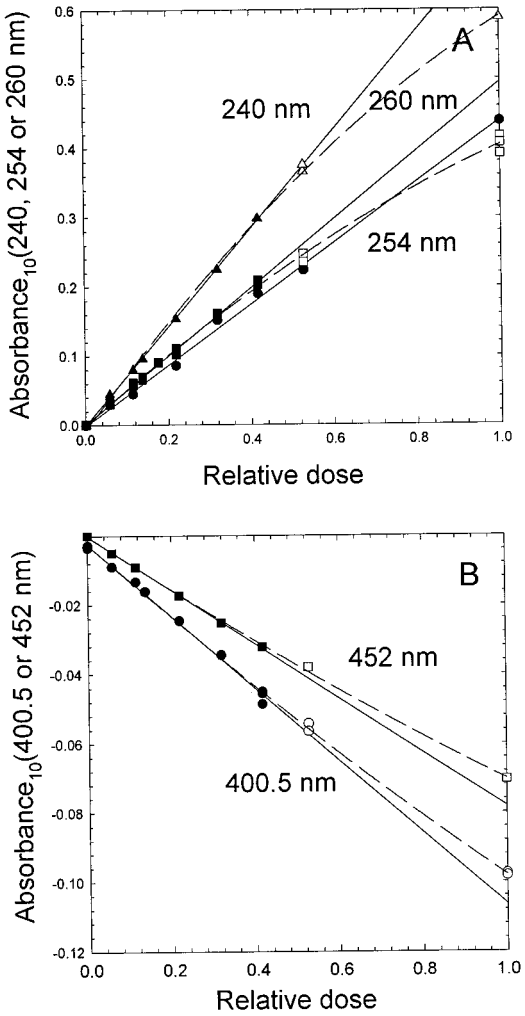

Figure 1. (A) Maximum transient absorptions versus radiolysis dose. Circles are data obtained using mixtures of 50 mbar of O_2, 950 mbar of CO_2, and a montoring wavelength of 254 nm. Squares are data obtained using mixtures of 10 mbar of CH_4, 40 mbar of O_2, 950 mbar of SF_6, and a montoring wavelength of 260 nm. Triangles are data obtained using mixtures of 10 mbar of CH_4, 40 mbar of O_2, 950 mbar of SF_6, and a montoring wavelength of 240 nm. (B) Absorbance loss at 452 nm (squares) and 400.5 nm (circles) as a function of dose following radiolysis of mixtures of 0.5 mbar of NO_2 and 1000 mbar of SF_6. An optical path length of 120 cm was used. The straight lines are linear regressions through the low-dose data (filled symbols). See text for details.

$\sigma_{400.5nm}(NO_2) = (6.5 \pm 0.65) \times 10^{-19}$ and $\sigma_{452\ nm}(NO_2) = (4.5 \pm 0.45) \times 10^{-19}$ cm^2 molecule^{-1},[16−19] the F-atom yield was determined to be $(3.25 \pm 0.33) \times 10^{15}$, $(3.14 \pm 0.32) \times 10^{15}$, $(3.07 \pm 0.33) \times 10^{15}$, and $(3.33 \pm 0.34) \times 10^{15}$ cm^{-3} at full dose and 1000 mbar SF_6. Quoted uncertainties reflect both statistical uncertainties in the slopes from Figure 1 and a 10% uncertainty in $\sigma(CH_3O_2)$ and $\sigma(NO_2)$. It is gratifying to note the good agreement among these four different determinations. In the following we choose to use an average of the four determinations with a 10% uncertainty, $[F]_0 = (3.20 \pm 0.32) \times 10^{15}$ cm^{-3}.

Reagents used were the following: 10−100 mbar CH_3CHO (>99.5%); 20−120 mbar O_2 (ultrahigh purity); 850−900 mbar CO_2 (>99.9%); 870−1000 mbar SF_6 (>99.9%); 0.29−0.71 mbar NO (>99.8%); 0.23−0.63 mbar NO_2 (>98%). All gases were used as received.

Four sets of experiments were performed using the pulse-radiolysis system. First, mixtures of CH_3CHO, O_2, NO, and CO_2 were radiolyzed and the formation of NO_2 was monitored

at 400.5 and 452 nm to provide measurements of k_2. Second, mixtures of CH_3CHO, O_2, NO_2, and CO_2 were radiolyzed and the decay of NO_2 was monitored at 400.5 and 452 nm to provide measurements of k_3. Third, k_2 was determined from the rate of formation of NO_2 using radiolysis of mixtures of CH_3CHO, O_2, NO, and SF_6 and detection wavelengths of 400.5 and 452 nm. Finally, k_3 was determined from the rate of decay of NO_2 upon radiolysis of $CH_3CHO/O_2/NO_2/SF_6$ mixtures using detection wavelengths of 400.5 and 452 nm.

2.2. FTIR Systems at Ford and NCAR. The experimental systems at Ford[14] and NCAR[15] are described elsewhere and only discussed briefly here. In both systems chemical analysis was performed using FTIR spectroscopy. Experiments at Ford were conducted at 293−308 K and 5.9−700 Torr total pressure of N_2/O_2 diluent. Experiments at NCAR were performed over the temperature range 240−295 K in 30−700 Torr total pressure of N_2/O_2 diluent. The system at Ford Motor Company consists of a 2-m-long, 140-L evacuable Pyrex chamber surrounded by 22 UV fluorescent lamps interfaced to a Mattson Instruments Inc. Sirius 100 FTIR spectrometer. The system at NCAR consists of a 47-L stainless steel reactor fitted with a quartz window at one end to allow photolysis using a filtered xenon arc lamp. A Bomem DA 3.01 FTIR spectrometer was interfaced to a Hanst-type optical arrangement mounted within the reaction cell. The path lengths for the analyzing infrared beam were 28 m (Ford) and 33 m (NCAR), the spectral resolutions were 0.25 cm^{-1} (Ford) and 0.1−0.5 cm^{-1} (NCAR), infrared spectra were derived from 32 (Ford) and 100−200 (NCAR) coadded interferograms.

Initial concentrations (and purities) of the gas mixtures used were 16−26 mTorr of CH_3CHO (>99%), 49−460 mTorr of chlorine (>99%), 29−100 mTorr of NO_x (>99%), and 5.9−700 Torr of O_2/N_2 (both >99.999%) diluent. Isotopically labeled $^{13}CH_3{}^{13}CHO$ was used as the reactant in the experiments at Ford. Nonlabeled acetaldehyde was used at NCAR. Products were quantified by fitting reference spectra of the pure compounds obtained at appropriate total pressures to the observed product spectra using integrated absorption features. The procedure was as follows. The CH_3CHO, NO, and NO_2 reactants were quantified and subtracted from the product spectra using characteristic absorption features over the wavelength regions 800−1500 cm^{-1}. CO_2 and $CH_3C(O)O_2NO_2$ were then identified and quantified using features at 2000−2400 and 800−1500 cm^{-1}, respectively. With the exception of $CH_3C(O)O_2NO_2$, all reagent and reference compounds were obtained from commercial sources. Reference spectra of $CH_3C(O)O_2NO_2$ and $^{13}CH_3{}^{13}C(O)O_2NO_2$ were obtained by irradiation of acetaldehyde/$Cl_2/NO_2/O_2$ mixtures and equating the resulting peroxyacetyl nitrate features to the loss of acetaldehyde (corrected for a small, <2%, formation of CO_2 caused by the unavoidable presence of a small amount of NO in the reaction system). At 1163 cm^{-1} $\sigma(CH_3C(O)O_2NO_2) = 1.47 \times 10^{-18}$ cm^2 $molecule^{-1}$ while at 1133 cm^{-1} $\sigma(^{13}CH_3{}^{13}C(O)O_2NO_2) = 1.21 \times 10^{-18}$ cm^2 $molecule^{-1}$.[20]

3. Results

3.1. Absolute Rate Constant for the Reaction of $CH_3C(O)O_2$ Radicals with NO Using O Atom Initiation. The formation of NO_2 was studied by monitoring the absorbance at 400.5 and 452 nm following the radiolysis (full dose) of mixtures of 0.30−0.71 mbar of NO, 50 mbar of O_2, 75−100 mbar of CH_3CHO, and 850−875 mbar of CO_2. Figure 2 shows five absorption transients obtained using a detection wavelength of 400.5 nm. The maximum transient absorption at 400.5 and

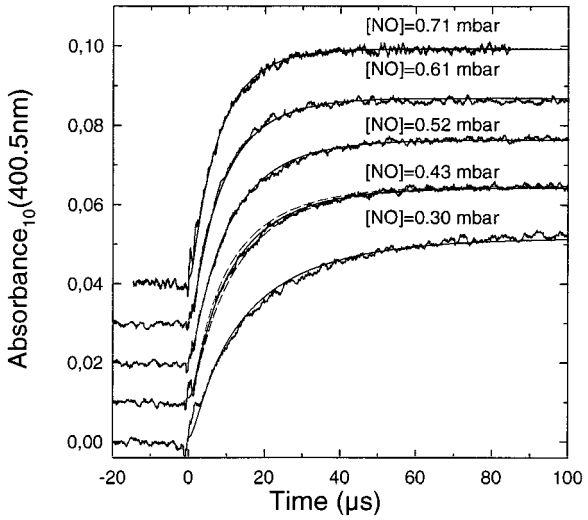

Figure 2. Absorption transients at 400.5 nm following pulsed radiolysis of mixtures of 0.30−0.71 mbar NO, 50 mbar O_2, 75−100 mbar CH_3CHO, and 850−875 mbar CO_2 (single pulses, full dose, and optical path length of 120 cm). For clarity, the transients are separated vertically by 0.01 units. The smooth solid lines are simulations using $k_2 = 2 \times 10^{-11}$ cm^3 $molecule^{-1}$ s^{-1}. Additional simulations of the transient where $[NO]_0 = 0.43$ mbar using $k_2 = 1.7 \times 10^{-11}$ and 2.3×10^{-11} cm^3 $molecule^{-1}$ s^{-1} are shown with smooth dashed lines.

452 nm was observed to scale in a fashion consistent with the absorption cross sections for NO_2 at these two wavelengths, $\sigma_{400.5\ nm}(NO_2) = 6.5 \times 10^{-19}$ and $\sigma_{452\ nm}(NO_2) = 4.5 \times 10^{-19}$ cm^2 $molecule^{-1}$.[16−19] In addition, the formation rate increased with increasing NO concentration (see Figure 2). It seems reasonable to assume that the observed absorption is caused by NO_2 formed from the following set of reactions:

$$CO_2 \xrightarrow{2\text{-MeV } e^-} CO + O \quad (5)$$

$$O + CH_3CHO \rightarrow CH_3CO + OH \quad (11)$$

$$OH + CH_3CHO \rightarrow CH_3CO + H_2O \quad (12)$$

$$CH_3CO + O_2 + M \rightarrow CH_3C(O)O_2 + M \quad (13)$$

$$CH_3C(O)O_2 + NO \rightarrow CH_3C(O)O + NO_2 \quad (2a)$$

$$CH_3C(O)O_2 + NO + M \rightarrow CH_3C(O)ONO_2 + M \quad (2b)$$

Consistent with previous work[8] and as discussed in section 3.6, we assume in the following that reaction 2b is unimportant and that $CH_3C(O)O$ radicals decompose immediately after their formation.

$$CH_3C(O)O + M \rightarrow CH_3 + CO_2 + M \quad (14)$$

The methyl radicals formed by reaction 14 add O_2 to give CH_3O_2 radicals that react with NO to produce another NO_2 molecule. Therefore, a first-order expression does not describe the NO_2 formation adequately, and the experimental transients need to be fitted using a chemical mechanism describing the chemical reactions in the system. To model the experimental absorption transients, the chemical mechanism shown in Table 1 and the absorption cross sections of NO_2 at 400.5 and 452 nm were applied. In addition, the absorption at 400.5 nm by CH_3ONO formed by the addition of CH_3O radicals to NO was included ($\sigma_{400.5\ nm}(CH_3ONO) = 1.7 \times 10^{-19}$ cm^2 $molecule^{-1}$ [21]). The chemical mechanism in Table 1 was constructed from the

TABLE 1: Reaction Mechanism Used To Fit the Experimental Data

reaction	rate constant (cm^3 $molecule^{-1}$ s^{-1})	ref
$O + CH_3CHO \rightarrow CH_3CO + OH$	4.5×10^{-13}	16
$O + O_2 + M \rightarrow O_3 + M$	3.1×10^{-14}	25
$O + NO + M \rightarrow NO_2 + M$	1.6×10^{-12}	16
$O + NO_2 + M \rightarrow 0.86NO + 0.86O_2 + 0.14NO_3 + M$	9.7×10^{-12}	16
$F + CH_3CHO \rightarrow CH_3CO + HF$	1.0×10^{-10}	28
$F + CH_3CHO \rightarrow HC(O)CH_2 + HF$	0.4×10^{-10}	28
$F + O_2 + M \rightarrow FO_2 + M$	1.9×10^{-13}	40
$F + NO + M \rightarrow FNO + M$	5.1×10^{-12}	41, 42
$F + NO_2 + M \rightarrow FNO_2 + M$	1.5×10^{-11}	43
$CH_3CHO + OH \rightarrow CH_3CO + H_2O$	1.6×10^{-11}	22
$NO + OH + M \rightarrow HONO + M$	4.8×10^{-12}	16
$NO_2 + OH + M \rightarrow HNO_3 + M$	1.1×10^{-11}	16
$CH_3CO + O_2 + M \rightarrow CH_3C(O)O_2 + M$	3.2×10^{-12}	26
$CH_3CO + NO + M \rightarrow CH_3C(O)NO + M$	2.6×10^{-11}	*a*
$CH_3CO + NO_2 + M \rightarrow CH_3C(O)NO_2 + M$	1.6×10^{-11}	*a*
$CH_3CO + CH_3CO + M \rightarrow CH_3C(O)C(O)CH_3 + M$	2.0×10^{-11}	44
$CH_3C(O)O_2 + CH_3C(O)O_2 \rightarrow 2CH_3 + 2CO_2 + O_2$	1.66×10^{-11}	22
$CH_3C(O)O_2 + NO \rightarrow CH_3 + CO_2 + NO_2$	2.0×10^{-11}	this work
$CH_3C(O)O_2 + NO_2 + M \rightarrow CH_3C(O)O_2NO_2 + M$	1.0×10^{-11}	this work
$CH_3C(O)O_2 + CH_3O_2 \rightarrow CH_3 + CO_2 + CH_3O + O_2$	5.5×10^{-12}	22
$CH_3C(O)O_2 + CH_3O_2 \rightarrow CH_3C(O)OH + HCHO + O_2$	5.5×10^{-12}	22
$CH_3 + O_2 + M \rightarrow CH_3O_2 + M$	1.07×10^{-12}	28
$CH_3 + NO + M \rightarrow CH_3NO + M$	1.04×10^{-11}	28
$CH_3 + NO_2 \rightarrow$ products	1.6×10^{-11}	*a*
$CH_3O_2 + NO \rightarrow CH_3O + NO_2$	7.7×10^{-12}	22
$CH_3O_2 + NO_2 + M \rightarrow CH_3O_2NO_2 + M$	7.5×10^{-12}	22
$CH_3O + NO + M \rightarrow CH_3ONO + M$	2.5×10^{-11}	16
$CH_3O + NO_2 + M \rightarrow CH_3ONO_2 + M$	1.7×10^{-11}	16
$O_3 + NO \rightarrow NO_2 + O_2$	1.8×10^{-14}	16
$NO + NO_3 \rightarrow NO_2 + NO_2$	2.6×10^{-11}	16
$NO_2 + NO_3 + M \rightarrow N_2O_5 + M$	1.3×10^{-12}	16
$CH_3CHO + NO_3 \rightarrow HNO_3 + CH_3CO$	2.4×10^{-15}	16
$HC(O)CH_2 + O_2 + M \rightarrow HC(O)CH_2O_2 + M$	2.6×10^{-13}	45
$HC(O)CH_2 + NO + M \rightarrow HC(O)CH_2NO + M$	2.5×10^{-11}	46
$HC(O)CH_2 + NO_2 + M \rightarrow HC(O)CH_2NO_2 + M$	1.9×10^{-11}	47
$HC(O)CH_2 + HC(O)CH_2 + M \rightarrow HC(O)CH_2CH_2CHO + M$	4.8×10^{-11}	*a*
$HC(O)CH_2O_2 + NO \rightarrow HC(O)CH_2O + NO_2$	8×10^{-12}	*a*
$HC(O)CH_2O_2 + NO_2 + M \rightarrow HC(O)CH_2O_2NO_2 + M$	6.4×10^{-12}	*a*
$2HC(O)CH_2O_2 \rightarrow 1.5HC(O)CH_2O + 0.25CHOCHO + 0.25HC(O)CH_2OH + O_2$	8×10^{-12}	*a*
$HC(O)CH_2O_2 + CH_3C(O)O_2 \rightarrow HC(O)CH_2O + CH_3 + CO_2 + O_2$	2.5×10^{-12}	*a*
$HC(O)CH_2O_2 + CH_3C(O)O_2 \rightarrow CHOCHO + CH_3C(O)OH + O_2$	2.5×10^{-12}	*a*
$HC(O)CH_2O_2 + CH_3O_2 \rightarrow HC(O)CH_2O + CH_3O + O_2$	1.1×10^{-12}	*a*
$HC(O)CH_2O_2 + CH_3O_2 \rightarrow$ stable products	2.7×10^{-12}	*a*
$HC(O)CH_2O + NO \rightarrow$ stable products	2.5×10^{-11}	*b*
$HC(O)CH_2O + NO_2 \rightarrow$ stable products	1.7×10^{-11}	*b*

[a] Assumed equal to the analogous reactions for the acetonyl radical $CH_3C(O)CH_2$.[48,49] [b] Assumed equal to $k(CH_3O + NO)$ and $k(CH_3O + NO_2)$.

literature data where available. The rate constants not available in the literature were obtained as follows. It was assumed that the rate constants for the reactions of CH_3CO radicals with NO and NO_2, the reaction of CH_3 radicals with NO_2, the self-reactions of CH_3CO, $HC(O)CH_2$, and $HC(O)CH_2O_2$ radicals and the cross reactions of $HC(O)CH_2O_2$ radicals with $CH_3C(O)O_2$ and CH_3O_2 radicals are equal to the rate constants for the analogous reactions of $CH_3C(O)CH_2$ radicals. In addition, the distribution between molecular and radical products from these reactions was estimated from the product distribution of the analogous $CH_3C(O)CH_2$ reaction. Finally, it was assumed that the rate constants for the reactions of $HC(O)CH_2O$ radicals with NO and NO_2 are equal to the reactions of CH_3O radicals with NO and NO_2.

Using this mechanism, we modeled the experimental transients in Figure 2 with k_2 varied to give the best fit. As seen from Figure 2, use of $k_2 = 2.0 \times 10^{-11}$ reproduces the experimental data well. To illustrate the sensitivity of the modeled transients to k_2, we present simulated transients obtained using $k_2 = 1.7 \times 10^{-11}$ and 2.3×10^{-11} cm^3 $molecule^{-1}$ s^{-1} (for [NO] = 0.43 mbar) in Figure 2. Use of $k_2 = 1.7 \times 10^{-11}$ and 2.3×10^{-11} gives transients in which the formation of NO_2 is too slow or too fast.

In addition to reaction 2 there are several other reactions that can potentially influence the kinetics of NO_2 formation that we need to consider. First, the rate of formation of $CH_3C(O)O_2$ radicals can obviously impact the observed rate of NO_2 formation. Under our experimental conditions the pseudo-first-order rates of formation of CH_3CO radicals (from reaction 11), $CH_3C(O)O_2$ radicals (from reaction 13), and NO_2 (via reaction 2) are $(0.83-1.1) \times 10^6$ s^{-1}, 3.9×10^6 s^{-1}, and $(1.5-3.5) \times 10^5$ s^{-1}. Clearly, the formation of NO_2 is not sensitive to the rate constant for the addition reaction of O_2 to the CH_3CO radical. However, it is not possible to avoid some dependency of the derived rate constant k_2 on the value used for the $O + CH_3CHO$ reaction. For this reason separate experiments were performed in which the reaction of F atoms with CH_3CHO was used as a source of CH_3CO radicals. As discussed in section 3.3, the value of k_2 determined in these separate experiments was indistinguishable from that presented in the present section.

Second, the formation of NO_2 is also dependent on the rate constant for the reaction of CH_3O_2 with NO. Fortunately, the rate constant for this reaction is well established.[16,22−24] It mainly influences the formation rate of the last part of the NO_2 transient while k_2 determines the formation rate of NO_2 just after the electron pulse. Consequently, the $CH_3C(O)O_2$ + NO and CH_3O_2 + NO reactions are partially separated in time.

Third, CH_3O radicals are formed in the reaction of CH_3O_2 with NO. Under the present experimental conditions the fate of CH_3O radicals is addition to either NO or NO_2 to give CH_3ONO or CH_3ONO_2. CH_3ONO has a small, but significant, absorption at the wavelengths used to monitor NO_2 formation. CH_3ONO_2 does not absorb in the region 400−450 nm.[21] The absorption associated with the formation of CH_3ONO was included in the model using an absorption cross section of 1.7×10^{-19} cm^2 molecule^{-1} [21] at 400.5 nm. At 452 nm the absorption due to CH_3ONO is negligible.[21] Finally, the value of the rate constant for the self-reaction of $CH_3C(O)O_2$ radicals, 1.6×10^{-11} cm^3 molecule^{-1} s^{-1}, also affects the measurements. The half-life for the self-reaction between $CH_3C(O)O_2$ radicals is $t_{1/2} = 1/(2k[CH_3C(O)O_2]) = 52$ μs (calculated using an average concentration of $CH_3C(O)O_2$ radicals $[CH_3C(O)O_2] \approx 0.6 \times 10^{15}$ cm^{-3}). The half-life for the reaction of $CH_3C(O)O_2$ radicals with NO is 2−5 μs, at least an order of magnitude faster than the self-reaction. Therefore, the influence of the self-reaction of $CH_3C(O)O_2$ is small. A simulation using [NO] = 0.43 mbar and the kinetic model in Table 1 shows that 7% of the $CH_3C(O)O_2$ radicals are removed by the self-reaction.

In summary, although the mechanism used to model the experimental data (see Table 1) is complex, reaction 2 is the key reaction that determines the rate of NO_2 formation. Other reactions play a minor role, and the influence of these reactions is explicitly taken into account. As seen in Figure 2, using $k_2 = 2.0 \times 10^{-11}$ cm^3 molecule^{-1} s^{-1} gives a good fit to experimental transients obtained using a range of NO concentrations. Also shown in Figure 2 are numerical simulations using $k_2 = 1.7 \times 10^{-11}$ and 2.3×10^{-11} cm^3 molecule^{-1} s^{-1}, which are well outside the error limits of the experiment. In light of the number of experimental absorption transients (nine) that are well fitted using $k_2 = 2.0 \times 10^{-11}$ cm^3 molecule^{-1} s^{-1} and the relatively well-established kinetic mechanism used for the simulations, we choose to quote a final value of $k_2 = (2.0 \pm 0.3) \times 10^{-11}$ cm^3 molecule^{-1} s^{-1}.

3.2. Absolute Rate Constant for the Reaction of $CH_3C(O)O_2$ Radicals with NO_2 Using O-Atom Initiation. The decay of NO_2 was studied by monitoring the absorbance at 400.5 and 452 nm following the radiolysis (full dose) of 0.235−0.58 mbar NO_2, 50 mbar of O_2, 100 mbar of CH_3CHO, and 850 mbar CO_2. Figure 3 shows typical absorption transients obtained using 400.5 nm as the detection wavelength. The decay rate increased with increasing NO_2 concentration. The absorption loss at 400.5 and 452 nm was observed to scale in a manner consistent with the absorption cross sections of NO_2 at these wavelengths. It seems reasonable to ascribe the observed loss of absorbance at 400.5 and 452 nm to loss of NO_2.

The chemical mechanism in Table 1 was used to model the experimental transients in Figure 3 with k_3 varied to give the best fit. As seen from Figure 3 the absorption transients were well fitted using $k_3 = 1 \times 10^{-11}$ cm^3 molecule^{-1} s^{-1}. To illustrate the sensitivity of the modeled transients to k_3, we present simulated transients obtained using $k_3 = 8 \times 10^{-12}$ and 12×10^{-12} cm^3 molecule^{-1} s^{-1} (for $[NO_2] = 0.305$ mbar) in Figure 3. The modeled transients using $k_3 = 8 \times 10^{-12}$ and 12 $\times 10^{-12}$ cm^3 molecule^{-1} s^{-1} fall well outside the noise level of the experimental absorption transients; hence, we report $k = (10 \pm 2) \times 10^{-12}$ cm^3 molecule^{-1} s^{-1}.

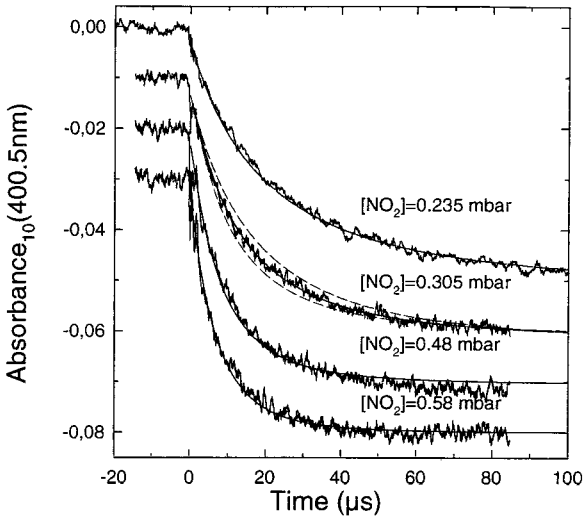

Figure 3. Absorption transients obtained at 400.5 nm following pulsed radiolysis of mixtures of 0.235−0.58 mbar NO_2, 50 mbar O_2, 100 mbar CH_3CHO, and 850 mbar CO_2 (single pulses, full dose, and optical path length of 120 cm). The smooth solid lines are simulations using $k_3 = 1 \times 10^{-11}$ cm^3 molecule^{-1} s^{-1}. Additional simulations of the transient where $[NO_2]_0 = 0.305$ mbar using $k_3 = 0.8 \times 10^{-11}$ and 1.2×10^{-11} cm^3 molecule^{-1} s^{-1} are shown with smooth dashed lines.

Several reactions could potentially interfere with the above determination of k_3. First, the O atoms may react with species other than CH_3CHO. O atoms generated by the radiolysis pulse can react via the following reactions:

$$O + CH_3CHO \rightarrow CH_3CO + OH \quad (11)$$

$$O + O_2 + M \rightarrow O_3 + M \quad (15)$$

$$O + NO_2 \rightarrow NO + O_2 \quad (16a)$$

$$O + NO_2 + M \rightarrow NO_3 + M \quad (16b)$$

For our experimental conditions with $[O_2] = 50$ mbar, $[NO_2] = 0.235-0.58$ mbar, and $[CH_3CHO] = 100$ mbar and using rate constants of $k_{11} = 4.5 \times 10^{-13}$,[16] $k_{15} = 3.1 \times 10^{-14}$,[25] $k_{16a} = 9.7 \times 10^{-12}$,[16] and $k_{16b} = 1.6 \times 10^{-12}$ cm^3 molecule^{-1} s^{-1}, [16] we calculate that >85% of the O atoms react to give CH_3CO and OH radicals, <3% of the O atoms are converted into O_3, <1.7% of the O atoms are converted into NO_3, and <10.6% of the O atoms are converted into NO. The small amounts of ozone, NO, and NO_3 produced by reactions 15 and 16 are not expected to complicate the study of reaction 3.

Second, CH_3CO radicals formed via reactions 11 or 12 can react with either O_2 or NO_2:

$$CH_3CO + O_2 + M \rightarrow CH_3C(O)O_2 + M \quad (13)$$

$$CH_3CO + NO_2 + M \rightarrow CH_3C(O)NO_2 + M \quad (17)$$

The rate constant for reaction 13 is 3.2×10^{-12} cm^3 molecule^{-1} s^{-1}.[26] There are no available data for reaction 17 at higher pressures. Assuming that the rate constant for reaction 17 is equal to that for the reaction between CH_3COCH_2 radicals and NO_2 of 2.6×10^{-11} cm^3 molecule^{-1} s^{-1}, we calculate that <9.1% of the CH_3CO radicals react via reaction 17 and that >90.9% of the CH_3CO radicals form $CH_3C(O)O_2$. Since

reaction 17 only consumes a small fraction of the CH_3CO radicals and since $CH_3C(O)NO_2$ is a closed-shell molecule, the formation of this species is not expected to interfere with this study.

Third, the formation rate of $CH_3C(O)O_2$ may influence the decay rate of NO_2. The pseudo-first-order rate constants for formation of CH_3CO and $CH_3C(O)O_2$ and for loss of NO_2 (from $CH_3C(O)O_2 + NO_2$) are 1.1×10^6, 3.9×10^6, and $(0.58-1.4) \times 10^5$ s^{-1}. Hence, the NO_2-loss rate is mainly dependent on k_3 with only minor influences from k_{12} and k_{15}.

Fourth, some $CH_3C(O)O_2$ radicals will undergo self-reaction leading to formation of CH_3 radicals, CO_2, and O_2. The half-life for the self-reaction between $CH_3C(O)O_2$ radicals is $t_{1/2} = 1/(2k[CH_3C(O)O_2]) = 52$ μs using an average concentration of $CH_3C(O)O_2$ radicals, $[CH_3C(O)O_2] \approx 0.6 \times 10^{15}$ cm^{-3}. The half-life for the reaction of $CH_3C(O)O_2$ radicals with NO_2 is 5−12 μs or 5−10 times faster than the self-reaction of $CH_3C(O)O_2$ radicals. The CH_3 radicals formed by the self-reaction will either react with O_2 to give CH_3O_2 radicals (which will react with NO_2) or react directly with NO_2. Both reactions lead to loss of another NO_2. The impact of the self-reaction of $CH_3C(O)O_2$ radicals is a slower overall decay of NO_2 since the loss of NO_2 is delayed. Self-reaction is the fate of up to 25% of the $CH_3C(O)O_2$ radicals. As seen in Figure 3, the chemical mechanism in Table 1 with $k_3 = 1.0 \times 10^{-11}$ provides a good fit for transients observed in the presence of 0.235−0.58 mbar of NO_2. The importance of the self-reaction as a loss of $CH_3C(O)O_2$ radicals varies by a factor of 2.5 over this range of $[NO_2]$, while the quality of the fits is unchanged, suggesting that the mechanism used here provides an adequate account of the $CH_3C(O)O_2$ radical self-reaction. We choose to report $k_3 = (1.0 \pm 0.2) \times 10^{-11}$ cm^3 $molecule^{-1}$ s^{-1} as determined above.

3.3. Absolute Rate Constant for the Reaction of $CH_3C(O)O_2$ Radicals with NO Using F-Atom Initiation. The formation of NO_2 was studied by monitoring the absorbance at 400.5 and 452 nm following the radiolysis (53% of full dose) of gas mixtures of 0.29−0.61 mbar of NO, 50 mbar of O_2, 10 mbar of CH_3CHO, and 940 mbar of SF_6. Figure 4 shows four absorption transients obtained at 400.5 nm. The maximum transient absorption at 400.5 and 452 nm was observed to scale in a fashion consistent with the absorption cross sections for NO_2 at these two wavelengths, and the formation rate increased with increasing NO concentration. We attribute the observed increase in absorption to NO_2 formed by the reaction of peroxy radicals with NO. However, three peroxy radicals could be formed in the system. $CH_3C(O)O_2$ radicals are formed by the following reactions:

$$F + CH_3CHO \rightarrow CH_3CO + HF \qquad (18)$$

$$CH_3CO + O_2 + M \rightarrow CH_3C(O)O_2 + M \qquad (13)$$

From the rate constants in Table 1 and correcting the yield of $CH_3C(O)O_2$ radicals for small losses of CH_3CO radicals and F atoms due to reaction with NO, we calculate that 64−68% of the initially formed F atoms are converted into $CH_3C(O)O_2$ radicals. $HC(O)CH_2O_2$ radicals are formed by the reactions

$$F + CH_3CHO \rightarrow HC(O)CH_2 + HF \qquad (19)$$

$$HC(O)CH_2 + O_2 + M \rightarrow HC(O)CH_2O_2 + M \qquad (20)$$

Using the rate constants in Table 1, we calculate that 13−18% of the F atoms are converted to $HC(O)CH_2O_2$ radicals.

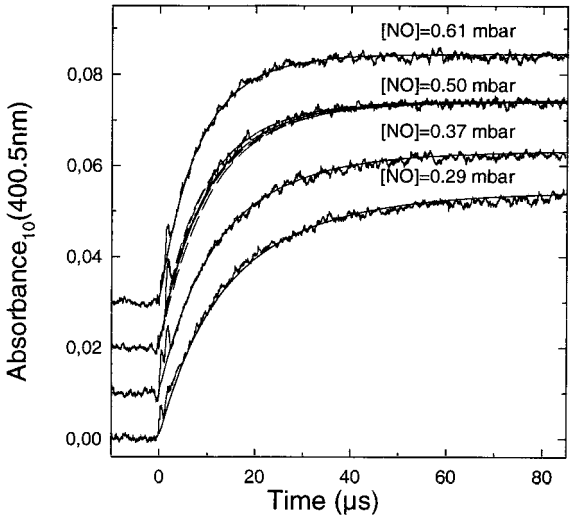

Figure 4. Absorption transients at 400.5 nm following pulsed radiolysis of mixtures of 0.29−0.61 mbar NO, 50 mbar O_2, 10 mbar CH_3CHO, and 940 mbar SF_6 (single pulses, 53% of full dose, and optical path length of 120 cm). For clarity, the transients are separated vertically by 0.01 units. The smooth solid lines are simulations using $k_2 = 2 \times 10^{-11}$ cm^3 $molecule^{-1}$ s^{-1}. Additional simulations of the transient where $[NO]_0 = 0.50$ mbar with $k(HC(O)CH_2O_2 + NO)$ varied by a factor of 2 (short-dashed lines, hardly distinguishable from the solid and the long-dashed lines) and $k_2 = 1.6 \times 10^{-11}$ and 2.4×10^{-11} cm^3 $molecule^{-1}$ s^{-1} are shown with smooth long-dashed lines.

In addition to these two peroxy radicals, CH_3O_2 radicals are formed via the following set of reactions:

$$CH_3C(O)O_2 + NO \rightarrow CH_3C(O)O + NO_2 \qquad (2a)$$

$$CH_3C(O)O + M \rightarrow CH_3 + CO_2 + M \qquad (11)$$

$$CH_3 + O_2 + M \rightarrow CH_3O_2 + M \qquad (9)$$

From the rate constants in Table 1 and neglecting radical−radical chemistry, we calculate a yield of CH_3O_2 radicals of 59−65% relative to the initial F-atom yield.

We have a mixture of three different peroxy radicals that can react with NO to produce NO_2. It is not possible to derive k_2 from a fit of an analytical expression to the experimental absorption transient; instead, it is necessary to model the absorption transient. The rate constant for the reaction of CH_3O_2 with NO is well-known and can be well represented in the model. However, the rate constant for the reaction of $HC(O)CH_2O_2$ radicals with NO is not known and the fate of the subsequently formed radical, $HC(O)CH_2O$, is unknown. In the following we have assumed that $k(HC(O)CH_2O_2 + NO) = k(CH_3C(O)CH_2O_2 + NO) = 8 \times 10^{-12}$ cm^3 $molecule^{-1}$ s^{-1}.[27] It was also assumed that $HC(O)CH_2O$ radicals are the only product of the reaction between $HC(O)CH_2O_2$ radicals and NO. The fate of $HC(O)CH_2O$ radicals in the system has been shown to be reaction with NO to give $HC(O)CH_2ONO$.[28] The experimental transients shown in Figure 4 were modeled using the mechanism given in Table 1 with $k(HC(O)CH_2O_2 + NO) = 8 \times 10^{-12}$ cm^3 $molecule^{-1}$ s^{-1}. The model reproduced the experimental absorption transients well. As a check of the sensitivity of the model to $k(HC(O)CH_2O_2 + NO)$, we modeled an absorption transient with $[NO]_0 = 0.50$ mbar, changing $k(HC(O)CH_2O_2 + NO)$, up and down by a factor of 2. The result is shown in Figure 4. The modeled curves are shown as smooth, short-dashed lines that can hardly be distinguished from the solid and long-dashed lines. We conclude that the result is not very

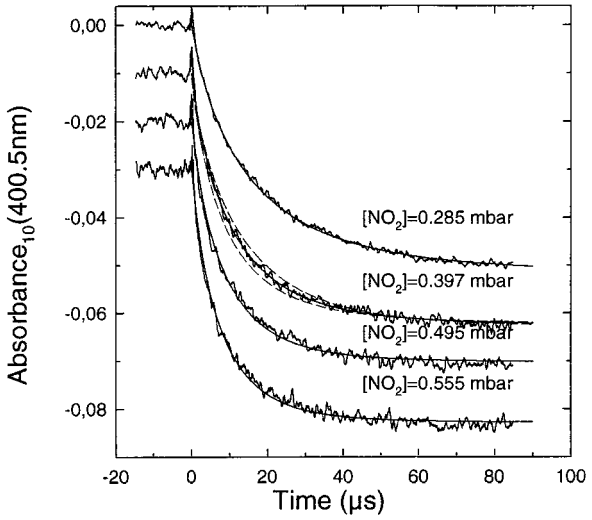

Figure 5. Absorption transients obtained at 400.5 nm following pulsed radiolysis of mixtures of 0.285−0.555 mbar NO_2, 50 mbar O_2, 10 mbar CH_3CHO, and 940 mbar SF_6 (single pulses, 53% of full dose, and optical path length of 120 cm). The smooth solid lines are simulations using $k_3 = 1 \times 10^{-11}$ cm^3 molecule^{-1} s^{-1}. Additional simulations of the transient where $[NO_2]_0 = 0.397$ mbar using $k_3 = 0.8 \times 10^{-11}$ and 1.2×10^{-11} cm^3 molecule^{-1} s^{-1} are shown with smooth dashed lines.

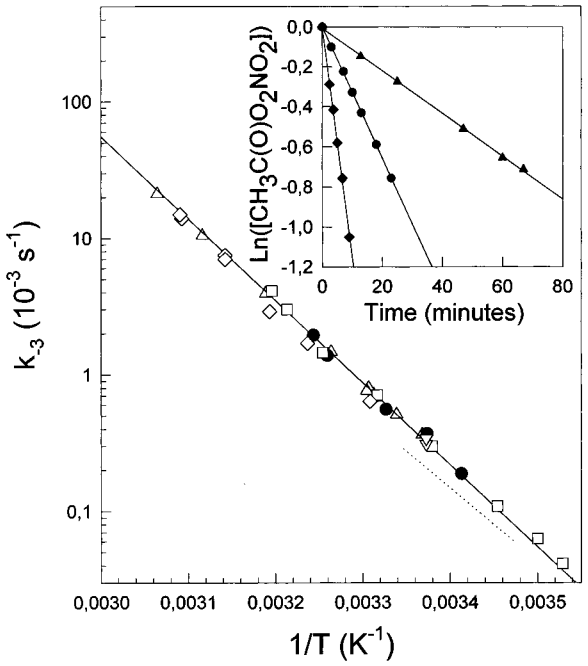

Figure 6. Arrhenius plot for k_{-3} at 700 (●) Torr total pressure of N_2 diluent. The solid line is a linear least-squares fit. Previous data for k_{-3} reported by Tuazon et al.[30] (at 740 Torr), Bridier et al.[5] (at 600 Torr), Roberts and Bertman[31] (at 760 Torr), Roumelis and Glavas[32] (at 760 Torr), and Grosjean et al.[33] (at 750 Torr) are indicated by the squares, triangles, diamonds, inverted triangles, and dotted line, respectively. The insert shows the observed decay of $CH_3C(O)O_2NO_2$ at 293.0 (triangles), 300.6 (circles), and 308.3 K (diamonds) in 700 Torr of N_2 diluent.

sensitive to $k(HC(O)CH_2O_2 + NO)$. We estimate the uncertainty in $k(CH_3C(O)O_2 + NO)$ due to uncertainty in $k(HC(O)CH_2O_2 + NO)$ to be 0.2×10^{-11} cm^3 molecule^{-1} s^{-1}.

Finally, as a check of the sensitivity of the model to $k(CH_3C(O)O_2 + NO)$, we modeled the absorption transient in Figure 4 with $[NO]_0 = 0.50$ mbar using $k(CH_3C(O)O_2 + NO) = 1.6 \times 10^{-11}$ and 2.4×10^{-11} cm^3 molecule^{-1} s^{-1}. The derived transients are shown in Figure 4 with long-dashed lines. As seen from Figure 4, the fits are sensitive to the value of $k(CH_3C(O)O_2 + NO)$. Eight experiments were well described by the model using $k(CH_3C(O)O_2 + NO) = 2.0 \times 10^{-11}$ cm^3 molecule^{-1} s^{-1}. From the F-atom-initiated experiments, we derive $k(CH_3C(O)O_2 + NO) = (2.0 \pm 0.5) \times 10^{-11}$ cm^3 molecule^{-1} s^{-1}; the quoted errors reflect both statistical uncertainties and our estimate of possible systematic uncertainties associated with $k(HC(O)CH_2O_2 + NO)$. This result is consistent with, although less precise than, that reported in section 3.1.

3.4. Absolute Rate Constant for the Reaction of $CH_3C(O)O_2$ Radicals with NO_2 Using F-Atom Initiation. The decay of NO_2 was studied by monitoring the absorbance at 400.5 and 452 nm following the radiolysis (53% of full dose) of mixtures of 0.285−0.63 mbar of NO_2, 50 mbar of O_2, 10 mbar of CH_3CHO, and 940 mbar of SF_6. Figure 5 shows typical absorption transients obtained at 400.5 nm. The decay rate increased with increasing NO_2 concentration. The absorption loss at 400.5 and 452 nm scaled with the absorption cross sections of NO_2 at these wavelengths. We ascribe the observed loss of absorbance to loss of NO_2 via reaction 3. The transients in Figure 5 were modeled using the mechanism given in Table 1. The best fits were achieved using $k_3 = 1.0 \times 10^{-11}$ cm^3 molecule^{-1} s^{-1} and are shown as the smooth curves.

Before the NO_2 loss rate can be used to determine the rate constant for reaction 3 we need to consider possible interfering reactions. As discussed in section 3.3, three different peroxy radicals are formed in the system. $CH_3C(O)O_2$ and $HC(O)CH_2O_2$ are produced following reaction of F atoms with CH_3CHO. CH_3O_2 radicals are formed following the self-reaction of $CH_3C(O)O_2$ radicals as discussed below. We estimate the yields of $CH_3C(O)O_2$ and $HC(O)CH_2O_2$ radicals to be 66−69% and 15−20% of the initial F-atom yield. The remaining F atoms are consumed by reaction with NO_2. Hence, 77−82% of the initially formed peroxy radicals are $CH_3C(O)O_2$ radicals. To simulate the observed absorption transient, we had to assume that $k(HC(O)CH_2O_2 + NO_2)$ is 6.4×10^{-12} cm^3 molecule^{-1} s^{-1} by analogy to $k(CH_3C(O)CH_2O_2 + NO_2)$.[27]

An additional complication is that the self-reaction of the $CH_3C(O)O_2$ radicals is relatively fast. Therefore, a nonnegligible fraction of the $CH_3C(O)O_2$ radicals undergoes self-reaction to give $CH_3C(O)O$ radicals that decompose to CH_3 radicals and CO_2. The half-life for the self-reaction between $CH_3C(O)O_2$ radicals is $t_{1/2} = 1/(2kC_{average}) = 52$ μs using an average concentration of $CH_3C(O)O_2$ radicals $C_{average} \approx 0.6 \times 10^{15}$ cm^{-3}. The half-life for the reaction of $CH_3C(O)O_2$ radicals with NO_2 is 5−10 μs or 5−10 times faster than the self-reaction of the $CH_3C(O)O_2$ radical. The CH_3 radicals formed by the self-reaction will react with NO_2 either directly or indirectly (via formation of CH_3O_2). Both reactions lead to loss of NO_2. The effect of the self-reaction of $CH_3C(O)O_2$ radicals is a slower overall decay of NO_2, since the loss of NO_2 is delayed. However, since the model can fit all absorption transients with different initial NO_2 concentrations and since it is possible to determine the fate of the products of the self-reaction of $CH_3C(O)O_2$ radicals, this reaction is a complication that can be dealt with.

Finally, we checked the sensitivity of the model to k_3. Figure 5 shows two dashed lines that are simulations of the experiment with $[NO]_0 = 0.397$ mbar using $k_3 = 8 \times 10^{-12}$ and 12×10^{-12} cm^3 molecule^{-1} s^{-1}. Clearly, these two simulations fall well outside the noise level of the transient. We choose to report $k_3 = (1.0 \pm 0.2) \times 10^{-11}$ cm^3 molecule^{-1} s^{-1}. This result is consistent with that reported in section 3.2.

TABLE 2: Measured Values for k_{-3}[a]

temp (K)	total pressure (Torr) (nitrogen diluent)	k_{-3} (10^{-3} s^{-1})
308.3	700	1.95 ± 0.14
306.8	700	1.38 ± 0.09
300.6	700	0.557 ± 0.031
296.4	700	0.371 ± 0.058
293.0	700	0.188 ± 0.010
293.1	100	0.162 ± 0.015
293.1	30	0.141 ± 0.014

[a] Quoted errors are two standard deviations.

3.5. Thermal Stability of $CH_3C(O)O_2NO_2$. As a preliminary exercise prior to measurement of k_2/k_3, control experiments were performed to measure the thermal stability of $CH_3C(O)O_2NO_2$. To check for heterogeneous loss of $CH_3C(O)O_2NO_2$ in the chamber at Ford, a mixture of $CH_3C(O)O_2NO_2$ in the presence of a large excess of NO_2 was left in the chamber in the dark for 64 min at 308 K. There was no loss (<2%) of $CH_3C(O)O_2NO_2$, suggesting the absence of complications caused by heterogeneous loss processes (PAN is known to be very stable in the NCAR chamber[29]). Addition of NO to reaction mixtures containing $CH_3C(O)O_2NO_2$ led to a decay of this species. In the presence of excess NO, the loss of $CH_3C(O)O_2NO_2$ was not dependent on the NO concentration. The loss of $CH_3C(O)O_2NO_2$ in the presence of NO is not caused by a reaction of these two compounds. Instead, NO scavenges $CH_3C(O)O_2$ radicals formed in the thermal decomposition of $CH_3C(O)O_2NO_2$, thereby limiting the re-formation of $CH_3C(O)O_2NO_2$ via reaction 3:

$$CH_3C(O)O_2NO_2 + M \rightarrow CH_3C(O)O_2 + NO_2 + M \quad (-3)$$

$$CH_3C(O)O_2 + NO_2 + M \rightarrow CH_3C(O)O_2NO_2 + M \quad (3)$$

$$CH_3C(O)O_2 + NO \rightarrow CH_3C(O)O + NO_2 \quad (2)$$

The decay of $CH_3C(O)O_2NO_2$ followed first-order kinetics. Representative data are shown in the insert in Figure 6. Linear least-squares analysis of these data gives pseudo-first-order rate constants for the thermal decomposition of $CH_3C(O)O_2NO_2$. $CH_3C(O)O_2NO_2$ can be regenerated via reaction 3. The observed rate of $CH_3C(O)O_2NO_2$ decay k_{obs} is related to the true rate of decay k_{-3} by the expression

$$k_{-3} = k_{obs}(1 + (k_3[NO_2]/k_2[NO]))$$

The observed $CH_3C(O)O_2NO_2$ decay rate k_{obs} was corrected for regeneration via reaction 3 using $k_3 = 1.0 \times 10^{-11}$ and $k_2 = 2.0 \times 10^{-11}$ cm^3 molecule^{-1} s^{-1} (see previous sections). The concentrations of NO and NO_2 in the chamber were monitored using their characteristic IR absorptions. Corrections were in the range 2−10% and have been applied to the data given in Table 2 and the Arrhenius plot in Figure 6.

Experiments were performed at a variety of temperatures over the range 293−308 K. Results are listed in Table 2 and plotted in Figure 6 together with previous measurements of k_{-3} by Tuazon et al.[30] at 740 Torr, Bridier et al.[5] at 600 Torr, Roberts and Bertman[31] at 760 Torr, Roumelis and Glavas[32] at 760 Torr, and Grosjean et al.[33] at 750 Torr. As seen from Figure 6, the results from the present work are in excellent agreement with all previous measurements except those of Grosjean et al.[33] which lie 20−30% below the rest of the data. To test for the effect of total pressure, experiments were performed at 293 K with 30, 100, or 700 Torr total pressure. As seen from Table 2, there was a small, but significant, effect of total pressure on k_{-3}. Reaction −3 is a unimolecular decomposition, and a decrease in k_{-3} with decreasing total pressure is to be expected. At 293 K the IUPAC data-evaluation panel recommends that when compared with the value at 700 Torr, the rate of PAN decomposition decreases by 12% and 35% at 100 and 30 Torr, respectively.[22] The dependence of k_{-3} on total pressure observed in the present work is indistinguishable from that recommended by the IUPAC panel. As expected, the observed pressure dependence of k_{-3} is indistinguishable from that of k_3 (see Figure 8).

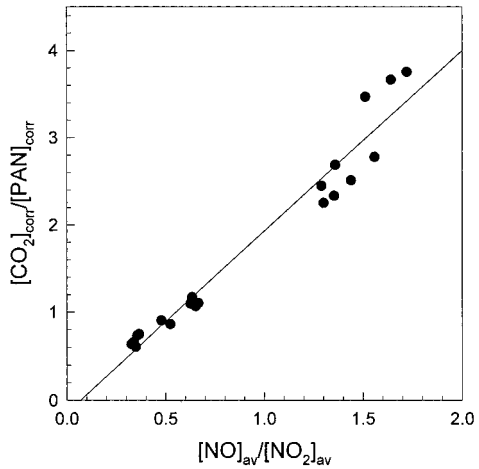

Figure 7. Plot of $\Delta[CO_2]_{corr}/\Delta[PAN]_{corr}$ versus $[NO]_{av}/[NO_2]_{av}$ at 700 Torr total pressure and 295 K. See text for details.

3.6. Measurement of k_2/k_3 at Ford and NCAR. The rate constant ratio k_2/k_3 was measured using the FTIR systems at Ford and NCAR in experiments employing the UV irradiation of acetaldehyde/Cl_2/NO/NO_2/O_2/N_2 mixtures.

$$Cl_2 + h\nu\ (\lambda > 300\ nm) \rightarrow 2Cl \quad (21)$$

$$Cl + CH_3CHO \rightarrow CH_3C(O) + HCl \quad (22)$$

$$CH_3C(O) + O_2 + M \rightarrow CH_3C(O)O_2 + M \quad (13)$$

Acetylperoxy radicals are formed via the reactions given above and then react with either NO or NO_2. As discussed above, reaction with NO leads to the formation of CO_2 while reaction with NO_2 produces peroxyacetyl nitrate (PAN). The relative importance of reactions 2 and 3 as loss mechanisms for $CH_3C(O)O_2$ radicals depends on the concentration ratio [NO]/[NO_2] and the rate constant ratio k_2/k_3. Provided that reactions 2 and 3 are the sole sources of CO_2 and PAN and that there are no losses of these species, then

$$\frac{[CO_2]}{[PAN]} = \left(\frac{k_2}{k_3}\right) \times \left(\frac{[NO]}{[NO_2]}\right)$$

where [CO_2], [PAN], [NO], and [NO_2] are the concentrations of CO_2, PAN, NO, and NO_2 in the chamber and k_2 and k_3 are the rate constants for reactions 2 and 3.

The first set of experiments was performed using the experimental system at Ford in 700 Torr of N_2 at 296 K using mixtures of 16−23 mTorr of $^{13}CH_3{}^{13}CHO$, 60 mTorr of Cl_2, 9−91 mTorr of NO, 22−56 mTorr of NO_2, and 200 Torr of O_2. Reaction mixtures were irradiated for 2−40 s, resulting in the loss of 2−24% of the initial $^{13}CH_3{}^{13}CHO$ and changes in the NO and NO_2 concentrations of 1−10%. In all cases the combined molar yields of CO_2 and PAN were indistinguishable from the observed acetaldehyde loss. Figure 7 shows a plot of

TABLE 3: Measured Values for k_2/k_3

temp (K)	total pressure (Torr) (nitrogen diluent)	k_2/k_3
295 (Ford data)	700	2.07 ± 0.21[a]
295 (Ford data)	300	2.38[b]
295 (Ford data)	100	2.70[b]
295 (Ford data)	50	3.36[b]
295 (Ford data)	25	3.12[b]
295 (Ford data)	5.9	5.46[b]
283 (NCAR data)	700	2.2 ± 0.2
283 (NCAR data)	30	2.9 ± 0.3
243 (NCAR data)	700	2.1 ± 0.2
243 (NCAR data)	100	2.4 ± 0.2

[a] Obtained from linear least-squares analysis of the data in Figure 7. [b] Single point determinations.

$[CO_2]/[PAN]$ versus $[NO]_{av}/[NO_2]_{av}$ for experiments conducted at 700 Torr and 295 K, where $[NO]_{av}$ and $[NO_2]_{av}$ are the average concentrations of NO and NO_2 during the experiment. As expected, there is a linear relationship between $[CO_2]/[PAN]$ and $[NO]_{av}/[NO_2]_{av}$. Linear least-squares analysis of the data in Figure 7 gives $k_2/k_3 = 2.17 \pm 0.15$.

Derivation of the rate-constant ratio k_2/k_3 relies on the assumption that CO_2 and PAN are formed solely as a result of reactions 2 and 3 and are not lost via any process. Although it is difficult to imagine other sources of PAN in the chamber, it is not difficult to imagine other sources of CO_2. A control experiment was performed in which a mixture of 24 mTorr of $^{13}CH_3{}^{13}CHO$, 77 mTorr of Cl_2, 35 mTorr of NO, and 84 Torr of O_2 in 700 Torr total pressure of N_2 diluent was subjected to four successive 10-s periods of UV irradiation, leading to 21% consumption of the acetaldehyde. The molar yield of $^{13}CO_2$ (relative to loss of acetaldehyde) was $95 \pm 8\%$; PAN was just detectable with a yield of 1−2%. The fact that the $^{13}CO_2$ yield was not significantly greater than 100% shows that there are no confounding sources of CO_2 in this chemical system. Although there are no possible loss mechanisms for CO_2 in the reactor there are several possible loss processes for PAN that need consideration. PAN can be lost via thermal decomposition (see previous section), heterogeneous reactions, and reaction with Cl atoms or OH radicals (OH radicals are formed in the system via reaction of HO_2 radicals with NO). As discussed in the previous section, there was no evidence for heterogeneous loss of PAN in the chamber systems. PAN reacts very slowly with both Cl atoms and OH radicals,[34] and such reactions will not be significant in the present work. Finally, the yields of CO_2 and PAN can be corrected for the thermal decomposition of PAN during the 1−5 min taken for UV irradiation and data acquisition using the value of $k_{-3} = 3.9 \times 10^{-4}$ s^{-1} reported in the previous section. Corrections were in the range 1−6% and have been applied to the data in Figure 7. Linear least-squares analysis of the data in Figure 7 gives $k_2/k_3 = 2.07 \pm 0.21$ at 700 Torr and 295 K. Additional experiments were performed at reduced total pressures at 295 K. The results of these single-point determinations are given in Table 3. On the basis of the data scatter evident in Figure 7, we estimate that the single-point determinations have an associated uncertainty of ±15%.

The increase in k_2/k_3 with decreasing pressure reflects a decrease in the association rate constant k_3 with decreasing pressure. There have been three studies of the effect of pressure on k_3.[5−7] The most comprehensive study is that of Bridier et al.[5] The current data have been converted to absolute values for k_3 by use of $k_2 = 2.0 \times 10^{-11}$ cm^3 molecule^{-1} s^{-1} measured here and by Villalta and Howard.[11] The data are shown in Figure 8 along with those of Bridier et al., and the fitted line to their data. The current data are indistinguishable from those

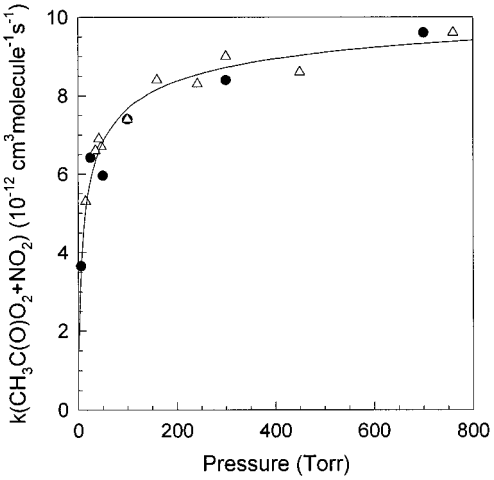

Figure 8. Pressure dependence for k_3 at 295 K measured in the present work (circles) and by Bridier et al.[5] (triangles).

of Bridier et al., and a nonlinear least-squares fit to the combined data set returns the same values of the parameters in the Troe expression: $k_o = 2.7 \times 10^{-28}$ and $k_{inf} = 1.2 \times 10^{-11}$ for $F_c = 0.3$ and $N_c = 1.41$.

Analogous experiments were performed at NCAR at 243 and 283 K for pressures between 30 and 700 Torr. For the initial experiments a resolution of 0.5 cm^{-1} was used. At the lower pressures the dependences of the absorption due to CO_2 and NO_2 became very nonlinear because of underresolution and saturation. The resolution was increased to 0.1 cm^{-1}, and concentrations were determined by the use of integrated line intensities rather than peak heights. This led to an improvement in the accuracy of measurements of these species. At the lowest temperature and pressure, the problem of CO_2 measurement was avoided by the measurement of CH_3ONO_2 instead of CO_2. At the low temperatures and low O_2 partial pressure, methyl nitrate is formed following the reaction of peroxyacetyl radicals with NO:

$$CH_3C(O)O_2 + NO \rightarrow CH_3 + CO_2 + NO_2 \quad (2)$$

$$CH_3 + O_2 + M \rightarrow CH_3O_2 + M \quad (9)$$

$$CH_3O_2 + NO \rightarrow CH_3O + NO_2 \quad (23)$$

$$CH_3O + NO_2 + M \rightarrow CH_3ONO_2 + M \quad (24)$$

The spectral features of methyl nitrate are smooth, and its concentration varied linearly with that of PAN over five or six irradiations.

The results are included in Table 3. When combined with the temperature dependence for the rate constant k_2 measured by Villalta and Howard,[11] the results at lower temperatures agree to within 5% with those predicted by the falloff parameters given by Bridier et al.,[5] further confirming the pressure dependence reported there. Because of the strong negative temperature dependence of k_3 at low pressure, measurements at low temperature do not extend very far into the falloff region, and so the paramaters for k_0 could not be improved.

4. Discussion and Conclusion

Recently, two groups have reported direct kinetic studies of the reaction of $CH_3C(O)O_2$ radicals with NO.[10,11] At room temperature (295−298 K) Villalta and Howard,[11] and Maricq and Szente[10] obtain values for k_2 of $(2.0 \pm 0.3) \times 10^{-11}$ and

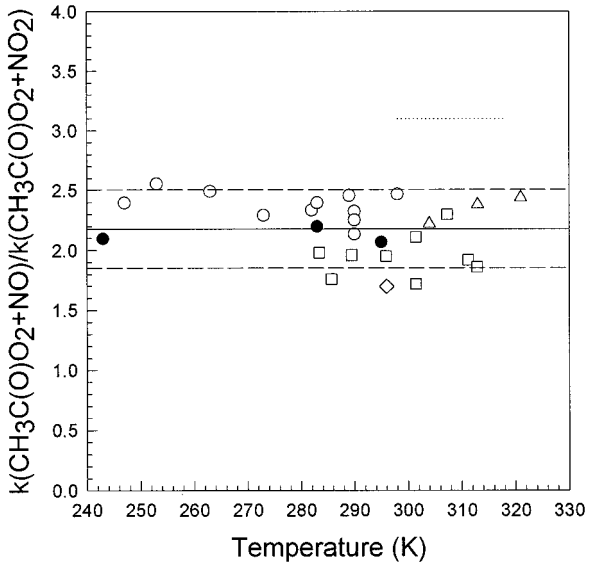

Figure 9. Comparison of literature data for k_2/k_3 at, or near, ambient pressure with results from the present work: Cox et al.[35] (diamond), Kenley and Hendry[38] (dotted line), Kirchner et al.[37] (triangles), Tuazon et al.[30] (squares), Seefeld et al.[39] (open circles), this work (filled circles). The solid line is drawn at $k_2/k_3 = 2.17$. The dashed line represent ±15%.

$(1.4 \pm 0.2) \times 10^{-11}$ cm^3 molecule^{-1} s^{-1}, respectively. Our value of $k_2 = (2.0 \pm 0.3) \times 10^{-11}$ cm^3 molecule^{-1} s^{-1} clearly supports the work of Villalta and Howard. Maricq and Szente[10] measured the formation of NO_2 and the loss of NO using IR and the formation and decay of $CH_3C(O)O_2$, CH_3O_2, and CH_3ONO using UV absorption. The experimental data were fitted using a complex mechanism; hence, the value of the rate-constant is obtained less directly than that of Villalta and Howard but in a way very similar to the work reported here. The origin of the discrepancy between the results of Maricq and Szente[10] and that measured here and by Villalta and Howard[11] is unknown.

Bridier et al.[5] determined a value for k_3 of 9.6×10^{-12} cm^3 molecule^{-1} s^{-1} at 1 bar total pressure and a high-pressure limit of $(1.2 \pm 0.2) \times 10^{-11}$ cm^3 molecule^{-1} s^{-1}. k_2 was determined at 1 bar total pressure of SF_6 or CO_2 in this work. SF_6 and CO_2 are generally more efficient third bodies than air, and it is expected from the results of Bridier et al.[5] that the value of k_3 determined here should lie between 0.96 and 1.2×10^{-11} cm^3 molecule^{-1} s^{-1}. This prediction is in excellent agreement with $k_3 = (1.0 \pm 0.2) \times 10^{-11}$ cm^3 molecule^{-1} s^{-1} obtained here. The rate-constant values of Addison et al.[6] and Basco and Parmar[7] fall below those obtained here and the values of Bridier et al. As discussed elsewhere,[8,9] the chemical mechanism used in the data analysis of Bridier et al.[5] was more complete than those used by Addison et al.[6] and Basco and Parmer.[7] Hence, the results of Bridier et al. are to be preferred. As seen in Figure 8, the results from the present study are in excellent agreement with those of Bridier et al.[5]

There have been six previous measurements of the rate-constant ratio k_2/k_3 at, or near, atmospheric pressure (Cox et al.,[35] Cox and Roffey,[36] Kirchner et al.,[37] Tuazon et al.,[30] Kenley and Hendry,[38] and Seefeld et al.[39]). Data from these previous studies are compared with the results from the present work in Figure 9. The data from Cox and Roffey[36] have a high degree of scatter with values ranging from 1.2 to 3.0 and are not included in the plot. All studies have concluded that the rate-constant ratio k_2/k_3 is independent of temperature. With the exception of the study of Hendry and Kenley[38] there is also broad agreement on the magnitude of k_2/k_3. The solid line in Figure 9 is drawn at $k_2/k_3 = 2.17$ which is the average of the data reported by Cox et al.,[35] Kirchner et al.,[37] Tuazon et al.,[30] Seefeld et al.,[39] and the present study. The two dashed lines represent changes in k_2/k_3 by ±15% and encompass most of the experimental data.

In models of urban and regional air chemistry the rate-constant ratio k_2/k_3 is an important parameter that determines the formation of PAN. We recommend the use of a temperature-independent value of $k_2/k_3 = 2.17 \pm 0.33$ in such models. Although the rate-constant k_3 is pressure-dependent, for pressures near ambient the effect is modest with k_3 changing by less than 5% as the pressure is reduced from 700 to 300 Torr at 298 K. Hence, neglecting the effect of pressure on k_2/k_3 in urban and regional air-quality models is reasonable.

Acknowledgment. J.S. and O.J.N. thank the Commission of the European Communities for financial support. NCAR is partially supported by the National Science Foundation.

References and Notes

(1) Moortgat, G. K.; Veyret, B.; Lesclaux, R. *J. Phys. Chem.* **1989**, *93*, 2362.
(2) Moortgat, G. K.; Veyret, B.; Lesclaux, R. *Chem. Phys. Lett.* **1989**, *160*, 443.
(3) Roehl, C. M.; Bauer, D.; Moortgat, G. K. *J. Phys. Chem.* **1996**, *100*, 4038.
(4) Villenave, E.; Lesclaux, R. *J. Phys. Chem.* **1996**, *100*, 14372.
(5) Bridier, I.; Caralp, F.; Loirat, H.; Lesclaux, R.; Veyret, B.; Becker, K. H.; Reimer, A.; Zabel, F. *J. Phys. Chem.* **1991**, *95*, 3594.
(6) Addison, M. C.; Burrows, J. P.; Cox, R. A.; Patrick, R. *Chem. Phys. Lett.* **1980**, *73*, 283.
(7) Basco, N.; Parmar, S. *Int. J. Chem. Kinet.* **1987**, *19*, 115.
(8) Lightfoot, P. D.; Cox, R. A.; Crowley, J. N.; Destriau, M.; Hayman, G. D.; Jenkin, M. E.; Moortgat, G. K.; Zabel, F. *Atmos. Environ.* **1992**, *26*, 1805.
(9) Wallington, T. J.; Dagaut, P.; Kurylo, M. J. *Chem. Rev.* **1992**, *92*, 667.
(10) Maricq, M. M.; Szente, J. J. *J. Phys. Chem.* **1996**, *100*, 12380.
(11) Villalta, P. W.; Howard, C. J. *J. Phys. Chem.* **1996**, *100*, 13624.
(12) Hansen, K. B.; Wilbrandt, R.; Pagsberg, P. *Rev. Sci. Instrum.* **1979**, *50*, 1532.
(13) Sehested, J. Risø-R-804, 1994.
(14) Wallington, T. J.; Japar, S. M. *J. Atmos. Chem.* **1989**, *9*, 399.
(15) Shetter, R. E.; Davidson, J. A.; Cantrell, C. A.; Calvert, J. G. *Rev. Sci. Instrum.* **1987**, *58*, 1427.
(16) DeMore, W. B.; Sander, S. P.; Golden, D. M.; Hampson, R. F.; Kurylo, M. J.; Howard, C. J.; Ravishankara, A. R.; Kolb, C. E.; Molina, M. J. Jet Propulsion Laboratory Publication, 94-26; Pasadena, CA, 1994.
(17) Davidson, J. A.; Cantrell, C. A.; McDaniel, A. H.; Shetter, R. E.; Madronich, S.; Calvert, J. G. *J. Geophys. Res.* **1988**, *93*, 7105.
(18) Schneider, W.; Moortgat, G. K.; Tyndall, G. S.; Burrows, J. P. *J. Photochem. Photobiol.* **1987**, *40*, 195.
(19) Mérienne, M. F.; Jenouvrier, A.; Coquart, B. *J. Atmos. Chem.* **1995**, *20*, 281.
(20) Tsalkani, N.; Toupance, G. *Atmos. Environ.* **1989**, *23*, 1849.
(21) Finlayson-Pitts, B. J.; Pitts, J. J. N. *Atmospheric Chemistry*; John Wiley & Sons: New York, 1986.
(22) Atkinson, R.; Baulch, D. L.; Cox, R. A.; Hampson, R. F.; Kerr, J. A.; Troe, J. *J. Phys. Chem. Ref. Data* **1992**, *21*, 1125.
(23) Eberhard, J.; Howard, C. J. *J. Phys. Chem.* **1997**, *101*, 3360.
(24) Sehested, J.; Nielsen, O. J.; Wallington, T. J. *Chem. Phys. Lett.* **1993**, *213*, 257.
(25) Sehested, J.; Nielson, O. J.; Egsgaard, H.; Larsen, N. W.; Pedersen, T.; Christensen, L. K.; Wiegell, M. *J. Geophys. Res.* **1995**, *100*, 20979.
(26) Tyndall, G. S.; Orlando, J. J.; Wallington, T. J.; Hurley, M. D. *Int. J. Chem. Kinet.* **1997**, *29*, 655.
(27) Sehested, J.; Christensen, L. K.; Nielsen, O. J.; Bilde, M.; Wallington, T. J.; Schneider, W. F.; Orlando, J. J.; Tyndall, G. S. *Int. J. Chem. Kinet.*, in press.
(28) Sehested, J.; Christensen, L. K.; Nielsen, O. J.; Wallington, T. J. *Int. J. Chem. Kinet.*, submitted.
(29) Orlando, J. J.; Tyndall, G. S.; Calvert, J. G. *Atmos. Environ.* **1992**, *26A*, 3111.
(30) Tuazon, E. C.; Carter, W. P. L.; Atkinson, R. *J. Phys. Chem.* **1991**, *95*, 2434.
(31) Roberts, J. M.; Bertman, S. B. *Int. J. Chem. Kinet.* **1992**, *24*, 297.
(32) Roumelis, N.; Glavas, S. *Monatsh. Chem.* **1992**, *123*, 63.

(33) Grosjean, D.; Grosjean, E.; Williams, E. L., II. *J. Air Waste Manage. Assoc.* **1994**, *44*, 391.
(34) Mallard, W. G.; Westley, F.; Herron, J. T.; Hampson, R. F. *NIST Chemical Kinetics Database*, Version 6.0; NIST Standard Reference Data; NIST: Gaithersburg, MD, 1994.
(35) Cox, R. A.; Derwent, R. G.; Holt, P. M.; Kerr, J. A. *Faraday Trans.* **1976**, 2061.
(36) Cox, R. A.; Roffey, M. J. *Environ. Sci. Technol.* **1977**, *11*, 900.
(37) Kirchner, F.; Zabel, F.; Becker, K. H. *Bunsenges. Phys. Chem.* **1990**, *94*, 1379.
(38) Kenley, R. A.; Hendry, D. G. *J. Am. Chem. Soc.* **1982**, *104*, 220.
(39) Seefeld, S.; Kinnison, J.; Kerr, J. A. *J. Phys. Chem.* **1997**, *101*, 55.
(40) Ellermann, T.; Sehested, J.; Nielsen, O. J.; Pagsberg, P.; Wallington, T. J. *Chem. Phys. Lett.* **1994**, *218*, 287.
(41) Sehested, J.; Ellermann, T.; Nielsen, O. J.; Wallington, T. J. *Int. J. Chem. Kinet.* **1994**, *26*, 615.
(42) Wallington, T. J.; Ellermann, T.; Nielsen, O. J.; Sehested, J. *J. Phys. Chem.* **1994**, *98*, 2346.
(43) Pagsberg, P.; Sillesen, A.; Jodkowski, J. T.; Ratajczak, E. *Chem. Phys. Lett.* **1996**, *252*, 165.
(44) Tsang, W.; Hampson, R. F. *J. Phys. Chem. Ref. Data* **1986**, *15*, 1087.
(45) Lorenz, K.; Rhäsa, D.; Zellner, R.; Fritz, B. *Ber. Bunsen-Ges. Phys. Chem.* **1985**, *89*, 341.
(46) Gutman, D.; Nelson, H. H. *J. Phys. Chem.* **1983**, *87*, 3902.
(47) Barnhard, K. J.; Santiago, A.; He, M.; Asmar, F.; Weiner, B. R. *Chem. Phys. Lett.* **1991**, *178*, 150.
(48) Bridier, I.; Veyret, B.; Lesclaux, R.; Jenkin, M. E. *J. Chem. Soc., Faraday Trans.* **1993**, *89*, 2993.
(49) Cox, R. A.; Munk, J.; Nielsen, O. J.; Pagsberg, P.; Ratajczak, E. *Chem. Phys. Lett.* **1990**, *173*, 206.